Switching-based Adaptive Active Noise Control for Periodic Signal with Unknown Path Model

Yang Wang *Member, IEEE*, Chengxi Zhong, Jiangkun Xu and Song Liu *Member, IEEE*

***Abstract*—In this letter, we present a novel switching-based adaptive feedback controller aiming to attenuate the multi-sinusoidal noises without priori knowledge about path model. Different from conventional approaches predominantly relying on filter-based methodologies, we conceptualize the Active Noise Control (ANC) system through the lens of Output Regulation (OR) within a discrete time framework. Accordingly, we formulate an observer-based regulator to actively counteract the noise, leveraging the internal model principle to notably enhance the noise reduction performance (NRP). A significant challenge encountered in this endeavor arises from the absence of comprehensive information regarding the path model, encompassing its dimensionality, structure, and the value of parameter. To this end, we developed an online adaptive law to estimate the frequency response at the relevant frequencies based solely on information from the error microphone. Moreover, the convergence time of the controller is further shorten through the incorporation of a delicately designed switching mechanism. Experimental results highlight the efficient adaptive multi-sinusoidal noise cancellation performance with an average reduction of more than -30 dB in terms of amplitude.**

***Index Terms*—Active noise control (ANC), Disturbance attenuation, Output regulation, Adaptive control.**

I. Introduction

The active control of noises or disturbances [1] has achieved great success in modern robotics [2], industrial processes [3], and automation systems [4]. As a promising technique, active noise control (ANC) aims to mitigate unwanted noises by virtue of generating anti-noise sound waves that destructively interfere with coming-forth unwanted sound noises [5]. Despite the accomplishments so far, there still exist limitations when addressing intricate and unknown systems perturbed by an unmeasurable periodic noise source spanning multiple low frequencies, such as vehicle interior, construction site [6]–[8] and sinusoidal signals generated by rotating machines [9]. Additionally, the pivotal requisites of global convergence and noise reduction performance remain unsolved [10]. Thus, a critical demand arises for an effective ANC strategy that can achieve significant attenuation of periodic noises featuring arbitrary multiple-harmonic frequencies in a duct system without prior model knowledge.

This work was in part supported by the National Natural Science Foundation of China under Grant 62303321. (*Corresponding author: Song Liu.*)

C. Zhong, J. Xu are with the School of Information Science and Technology, ShanghaiTech University, Shanghai 201210, China (email: zhongchx, xujk@shanghaitech.edu.cn).

S. Liu and Y. Wang are with the School of Information Science and Technology, ShanghaiTech University, Shanghai 201210, China, and with Shanghai Engineering Research Center of Intelligent Vision and Imaging, Shanghai, China (e-mail: liusong, wangyang4@shanghaitech.edu.cn).

Under this demand, filter-based ANC approaches have been widely studied, which fall into feedforward methods [11] and feedback methods [12]. For feedforward methods, the least-mean-square (LMS) based filter [13] and its derivatives [14]–[17] are representative through dynamically adjusting filter coefficients to minimize the mean square error between the desired signal and the filter output, subsequently achieving anti-noise waves that attenuate the primary noise at a specified location. Their straightforward and understandable structures simplify the implementation. However, filter-based feedforward methods exhibit weaknesses, including the limited cancellation ability and the potential instability brought by the acoustic coupling between primary and secondary path [18]. Thus, prior knowledge or online identification of the transfer function of the secondary path is crucial [19]. Furthermore, the feedforward methods essentially require a reference microphone mounted near source noises (see Fig. 1).

Contrarily, filter-based feedback ANC methods operate independently of the reference microphone [20]–[23], resulting in significantly reduced implementation costs (see Fig. 1). Nonetheless, it's crucial to recognize their inherent limitations. Primarily, stability concerns persist, akin to those encountered with infinite impulse response (IIR) filters [24] and the imperfect secondary path estimation [25]. Another drawback is the 'waterbed effect' [26], where achieving NRP at specific frequencies within a feedback ANC system may lead to increased noise levels at other frequencies. Such limitations necessitate the recalibration or redesign of ANC systems for different applications, rendering the development of a universally applicable high-NRP (noise reduction performance) filtered-based ANC across all frequencies impractical. Furthermore, the aforementioned techniques often fall short in achieving high-NRP for periodic noise at specific frequencies, achieving only limited attenuation of around -10 to -20 dB [27].

Here, we introduce a novel switching-based adaptive feedback controller aimed at achieving significant NRP of multi-sinusoidal noises emanating from unmodeled system while ensuring asymptotic stability. Its adaptive nature enables precise alignment of noise sources at arbitrary locations without the need for path model, thereby bolstering resilience against unexpected shifts in source noise and error microphone. Moreover, we enhance the convergence rate of the controller through the incorporation of a novel switching mechanism. In the rest of this paper, Section II delineates the addressed problem; Section III outlines the proposed controller; and Section IV provides detailed experimental results. Due to the limited space, simulation and rigorous convergence analysis are presented as the supplementary information.

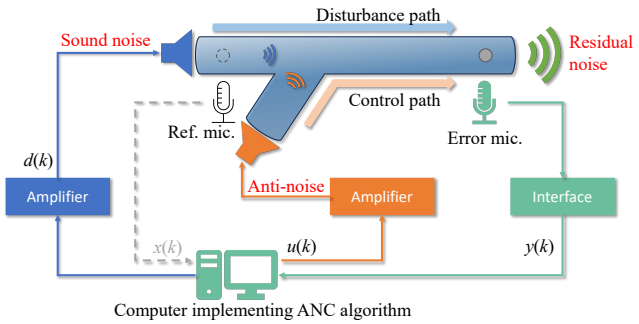

$d(k)$: disturbance signal; $u(k)$: control signal; $x(k)$: measured disturbance; $y(k)$: measured output.

Fig. 1: Standard ANC system with and without reference microphone.

II. Problem Statement

A. Standard ANC System

Figure 1 conceptually depicts the fundamental components of a standard ANC system, delineating two distinct pathways: the *Primary Path* from noise loudspeaker to error microphone, and the *Secondary Path* from anti-noise loudspeaker to error microphone. In this work, we focus on the feedback structure without a reference microphone. Specifically, the noise loudspeaker serves as an artificial noise generator, reproducing various sound noises with distinct characteristics. The anti-noise loudspeaker, acting as an actuator, delivers the algorithmically calculated anti-noise signal. The strategically positioned error microphone at the open end of the system collects residual noise, providing essential information for active noise control. Additionally, a computing platform generates noise signals, receives information collected by microphones, and generates anti-noise signals based on various ANC algorithms.

B. Mathematical Description of ANC System

In contrast to standard ANC separately modeling primary and secondary path [18], our ANC setup is viewed as a discrete linear time-invariant (LTI) single-input single-output (SISO) system, whose mathematical representation is expressed as:

$$\begin{aligned} x(k+1) &= Ax(k) + B\big[u(k) + d(k)\big] \\ y(k) &= Cx(k) \end{aligned} \tag{1}$$

where $x(k)$ is the *unmeasurable* state variables, $d(k)$, $u(k)$, and $y(k)$ are *unmeasurable* sound noise, anti-noise signal, and residual noise from error microphone. The sound propagation in the unknown duct system is modeled by the matrices A, B, and C, **whose explicit knowledge is completely unknown**.

Our primary objective is devising $u(k)$ to minimize undesirable $d(k)$ solely based on $y(k)$, without relying on matrices A, B, and C. The sound noise $d(k)$ examined here follows a specific pattern given as the following assumption:

Assumption 1: The sound noise $d(k)$ is formed by the combination of N distinct sinusoidal signals:

$$d(k) = \sum_{n=1}^{N} \psi_n \sin(\omega_n k + \phi_n), \tag{2}$$

each sinusoidal signal has a *known* frequency $\omega_n > 0$ with *unknown* amplitude and phase ($\psi_n > 0$, $\phi_n \in (-\pi, \pi]$). ◁

III. Switching-based Adaptive ANC

Our controller estimates the sound noise $d(k)$ and generates a signal $u(k)$ opposite to $d(k)$ to achieve high NRP. It aims to minimize the required system information while maintaining a relatively low dimension (which increases linearly with the number of noise frequencies). Thus, we build upon our earlier work [28] and introduce a new discrete-time switching-based adaptive active noise controller, outlined as:

$$\begin{aligned} u(k) &= \Gamma \hat{v}(k) \\ \hat{v}(k+1) &= S\hat{v}(k) - \varepsilon G \hat{\boldsymbol{\theta}}_\sigma^\top(k) \hat{\zeta}_o(k) \\ \hat{\zeta}_o(k+1) &= F_\varepsilon(k)\hat{\zeta}_o(k) - \alpha \Gamma^\top \big[\Gamma \hat{\zeta}_o(k) - y(k)\big] \end{aligned} \tag{3}$$

where $\hat{v}(k) \in \mathbb{R}^{2N}$ aims to estimate the sound noise $d(k)$. The estimation process inevitably induces estimation error. However, since the sound noise itself is not directly measurable, obtaining the estimation error is typically not possible. Thus, we introduce an observer denoted as $\hat{\zeta}_o(k) \in \mathbb{R}^{2N}$, which corrects the estimation error and drives it towards zero.

$\hat{\boldsymbol{\theta}}_\sigma(k)$ and $F_\varepsilon(k)$ in (3) will be explained later in (10), while S, G, and Γ are constant matrices defined as follows:

$$\begin{aligned} &S = \mathrm{diag}(S_1, \ldots, S_N),\ S_n = \begin{bmatrix} \cos\omega_n & \sin\omega_n \\ -\sin\omega_n & \cos\omega_n \end{bmatrix}, \\ &g = [1, 0]^\top,\ G = \mathrm{diag}(g, \ldots, g),\ \Gamma = [g^\top, \ldots, g^\top], \end{aligned} \tag{4}$$

where $\mathrm{diag}(\cdot)$ denotes the diagonal matrix operation. The parameters ε and α correspond to positive gains, and it is important to choose both of them to be sufficiently small.

*1) **Adaptive Law**:* According to the internal model principle [29], to completely cancel out the sound noise $d(k)$, it is imperative to gain information about the frequency response of system (1) at each frequency ω_n, where $n \in \mathcal{N} = \{1, 2, \ldots, N\}$, which is defined by:

$$\theta_n^\top(\omega_n) := \big[\mathrm{Re}\big(H(e^{j\omega_n})\big) \quad -\mathrm{Im}\big(H(e^{j\omega_n})\big)\big], \tag{5}$$

where $H(e^{j\omega_n}) = C(e^{j\omega_n} \cdot I - A)^{-1}B$, $\mathrm{Re}(\cdot)$ and $\mathrm{Im}(\cdot)$ denote the real and imaginary parts, respectively. Despite the essentiality of $\theta_n(\omega_n)$, given the path model unknown, obtaining accurate values of $\theta_n(\omega_n)$ beforehand is impossible. To address this issue, we introduce an online adaptive law to estimate the frequency response $\theta_n(\omega_n)$ at each frequency ω_n. The adaptive law utilizes the error between the expected canceling effect and the currently achieved canceling effect, which can be represented by:

$$\eta_n(k+1) = \eta_n(k) - \gamma \hat{\xi}_{1,n}(k)\big[\Gamma\hat{\zeta}_o(k) - y(k) - \textstyle\sum_{n=1}^{N} \tilde{\theta}_n^\top(k)\hat{\xi}_{1,n}(k)\big], \tag{6}$$

where $\eta_n(k)$ denotes the estimate of the frequency response $\theta_n(\omega_n)$ at each frequency ω_n, γ is a positive tuning gain, $\tilde{\theta}_n(k)$ will be defined later, and $\hat{\xi}_{1,n}(k)$ represents the $(2n-1)$-th and $2n$-th elements of the regressor signal $\hat{\xi}_1(k)$. The update equation for $\hat{\xi}_1(k+1)$ is given by:

$$\hat{\xi}_1(k+1) = F_\alpha^\top \hat{\xi}_1(k) - \varepsilon G \hat{\boldsymbol{\theta}}_\sigma^\top(k)\hat{\zeta}_o(k), \tag{7}$$

where $F_\alpha = S - \alpha\Gamma^\top\Gamma$ is a stable constant matrix.

*2) **Switching Mechanism**:* During the ANC process, $\eta_n(k)$ is a fast-updated signal, which may lead to instability issues if directly implemented in the controller. Therefore, to ensure

the stability of the closed-loop system, we devise a novel switching mechanism to replace $\eta_n(k)$ with a surrogate signal $\hat{\theta}_{\sigma_n(k)}$. First, we select M different points within the 2D plane as constant candidate estimates for each frequency response $\theta_n(\omega_n)$, denoted as $\hat{\theta}_m^\top = [\hat{\theta}_{m,1}, \hat{\theta}_{m,2}]$, where $m \in \mathcal{M} := \{1, 2, \ldots, M\}$. Next, at each time step k, we calculate the distance between the fast-updated estimate $\eta_n(k)$ and the constant estimate $\hat{\theta}_m$ as the monitoring signal $\pi_n^m(k)$:

$$\pi_n^m(k) = \|\eta_n(k) - \hat{\theta}_m\|, \ n \in \mathcal{N}, \ m \in \mathcal{M}. \tag{8}$$

Then, for each frequency ω_n, we select the candidate estimate $\hat{\theta}_m$ closest to $\eta_n(k)$ as the surrogate signal $\hat{\theta}_{\sigma_n(k)}$, combining them to form $\hat{\boldsymbol{\theta}}_\sigma(k)$. In rare scenarios where $\eta_n(k)$ may be equidistant from multiple candidate estimates, potentially leading to infinite fast switching, we propose a hysteresis modification on the switching logic $\sigma_n(k)$, expressed as:

$$\sigma_n(k) = \underset{\sigma_n(k^-), m}{\arg\min} \{\pi_n^m, \pi_n^{\sigma_n(k^-)} - h\}, \tag{9}$$

where $m \in \mathcal{M}\backslash\{\sigma_n(k^-)\}$, $\sigma_n(k^-)$ indicates the index of the candidate estimate selected at the previous time step, and h is a small positive parameter used to avoid infinite fast switching. The hysteresis logic demonstrates that if $\eta_n(k)$ has the minimum distance to multiple candidate estimates, we still maintain the candidate estimate selected previously.

Hence, $\hat{\boldsymbol{\theta}}_\sigma(k)$ and $F_\varepsilon(k)$ at time step k are given as:

$$\begin{aligned} \hat{\boldsymbol{\theta}}_\sigma(k) &= \mathrm{diag}(\hat{\theta}_{\sigma_1(k)}, \ldots, \hat{\theta}_{\sigma_N(k)}) \\ F_\varepsilon(k) &= S - \varepsilon \hat{\boldsymbol{\theta}}_\sigma(k) \hat{\boldsymbol{\theta}}_\sigma^\top(k) \end{aligned} \tag{10}$$

The $\tilde{\theta}_n(k) = \hat{\theta}_{\sigma_n(k)} - \eta_n(k)$ in (6) stands for the error signal between $\hat{\theta}_{\sigma_n(k)}$ and $\eta_n(k)$. The controller's initial conditions are set to zero, except for $\eta_n(0)$, which starts at a predetermined location. The candidate frequency response estimates $\hat{\theta}_m$ are uniformly distributed across the entire 2D plane.

IV. Experiments and Results

A. System Setup and Implementation Details

Figure 2 depicts the key components of our setup. We designed an acoustic duct module with separate paths to manage noise and anti-noise signals. The noise loudspeaker generates simulated noise, while the anti-noise loudspeaker produces an anti-noise. The computing device, based on a cRIO-9049 NI 8-channel controller featuring a 1.60 GHz quad-core CPU, 4 GB DRAM, and 16 GB storage, is for real-time control. Sampling is performed using an NI 9250 sound acquisition card with 2 channels and a synchronous sampling rate of 102.4 kS/s, capturing residual noise from error microphones. By transmitting the controller-optimized anti-noise signal, we achieve constructive interference at the target position, effectively canceling out noise from noise loudspeaker. The acoustic module is equipped with two error microphone positions, enabling path model variation by adjusting microphone placement. For our proposed controller, we set parameters ε, α, γ, and h to 0.01, 0.01, 0.02, and 0.1, while γ is adjusted to 0.005 for composite noise cancellation evaluation. The sampling time is set to 0.002 s.

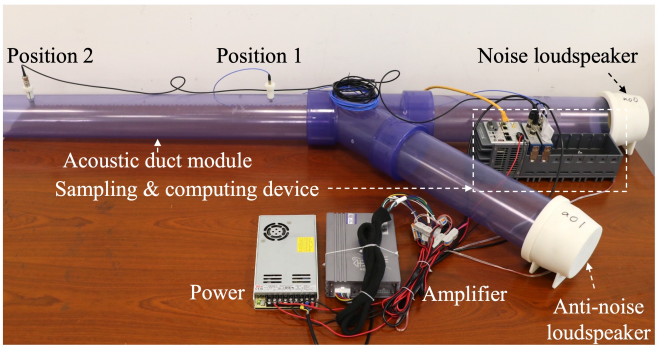

Fig. 2: The prototyped ANC system setup.

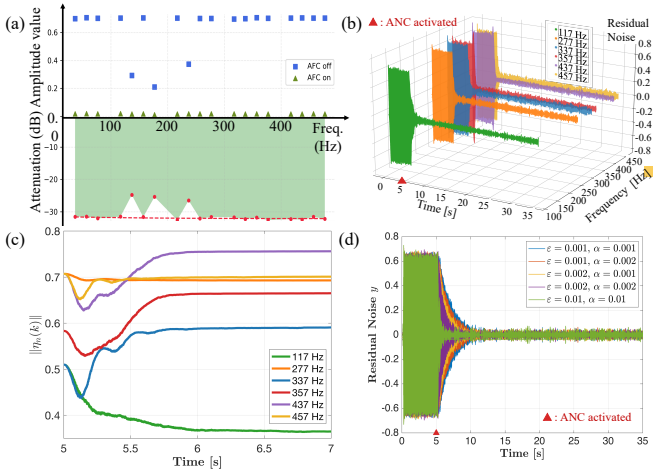

Fig. 3: Single frequency noise cancellation performance covering (a) that over the frequency spectrum, (b) efficacy (b) adaptive parameter convergence, (c) hyper-parameter effects.

B. Single Frequency Noise Cancellation

*1) **Noise Attenuation Efficacy**:* In Fig. 3 (a), we measured the initial noise amplitudes when AFC is off (royal blue squares) and residual noise amplitudes when AFC is on (olive green triangles) for distinct single frequencies. Additionally, the attenuation ability is quantified in decibels (dB) as $\mathrm{Att} = 20\log_{10}\left(\frac{\mathrm{Amp}_{\text{ANC on}}}{\mathrm{Amp}_{\text{ANC off}}}\right)$. We achieved an average attenuation of -30.95 dB. Furthermore, three notable frequencies (137 Hz, 177 Hz, and 237 Hz) exhibited consistent residual noise amplitudes compared to their initial noise levels, highlighting the stability of our controller irrespective of the initial noise amplitude. We also examined the noise reduction rates for distinct single-frequency noises. Fig. 3 (b) shows uniform noise reductions converging to nearly zero within approximately 5 seconds.

*2) **Convergence of the Adaptive Parameters**:* We visualized the trajectory of the adaptive signal norm, i.e. the estimate $\eta_n(k)$ of the frequency response of system (1) over different frequencies. Fig. 3 (c) shows $\eta_n(k)$ converged to a constant value for different frequencies, demonstrating our controller's adaptability to different ANC system and indicating the remaining residual noise in Fig. 3 (b) might be caused by measurement errors due to the limitations of microphone instead of algorithm convergence issues.

*3) **Hyper-Parameters Effects**:* In Fig. 3 (d), we explored the effects of key hyperparameters, ε and α, which respectively determine the optimization step size and the weight assigned to the regularization term. The evolution of residual noise y revealed that variations in ε and α influenced the convergence speed. Larger ε and higher α expedited the convergence process, resulting in faster noise reduction. Despite the influence on the convergence rate, these variations did not compromise the final noise suppression, highlighting the robustness of our controller in terms of varied hyperparameter settings.

*4) **Adaptability to Distinct Path Model**:* Different error microphone positions represent entirely duct systems with different path model. Despite this variability, our controller demonstrated a remarkable generality to distinct systems. By relocating the microphone from position 1 to position 2 in Fig. 2, a few single frequency noise cancellation experiments have been re-conducted, and the performance is summarized in Table I. Remarkably, the achieved suppression effects remained consistent after this repositioning. Thus, our controller is independent of the specific error microphone arrangement, demonstrating its robust adaptability to the unknown model.

TABLE I: Single frequency noise cancellation performance.

Freq. (Hz)	Before Att	After Att	Att (dB)
37	0.6995	0.0178	-31.8874
137	0.7000	0.0173	-32.1410
237	0.6986	0.0179	-31.8275
337	0.7000	0.0183	-31.6529
437	0.6987	0.0185	-31.5424

C. Composite Frequency Noise Cancellation

*1) **Noise Attenuation Efficacy**:* Next, we assessed the noise attenuation effectiveness of our controller for composite frequency noise comprising five distinct frequencies (67, 167, 267, 367, and 467 Hz) as illustrated in Fig. 4 (a). The results demonstrate that our controller successfully achieved effective noise attenuation for approximately 5 seconds, consistently maintaining a level of attenuation similar to that observed in the single-frequency case, approximately -31 dB.

*2) **Sequence of Switching Signals** $\hat{\theta}_{\sigma_n(k)}$:* Fig. 4 (b) illustrates the proposed switching mechanism by showcasing the switching process of the signal $\hat{\theta}_{\sigma_n(k)}$ for partial frequency components (167, 267, and 367 Hz). Since the actual position of the frequency response $\theta_n(\omega_n)$ is unknown due to the unknown model, only $\eta_n(k)$ at the final 25 seconds, is plotted. This figure demonstrates that $\hat{\theta}_{\sigma_n(k)}$ is selected and switched to $\hat{\theta}_m$ closest to $\eta_n(k)$. As $\eta_n(k)$ approaches the real frequency response $\theta_n(\omega_n)$, $\hat{\theta}_{\sigma_n(k)}$ continues to switch to $\hat{\theta}_m$ closest to the real frequency response.

*3) **SOTA Comparison**:* Finally, we compared our controller with FxLMS [30] and MAML [27] in handling composite frequency noise. The control filter and the secondary path estimate comprised 64 and 32 steps with a step size of 0.0002 and a sampling rate of 5 kHz. In Fig. 5, each radar line's extension in every frequency direction represented the attenuation (dB), while the area indicated the composite noise cancellation capability across all frequencies. FxLMS exhibited superior noise reduction capabilities in low-frequency scenarios, while

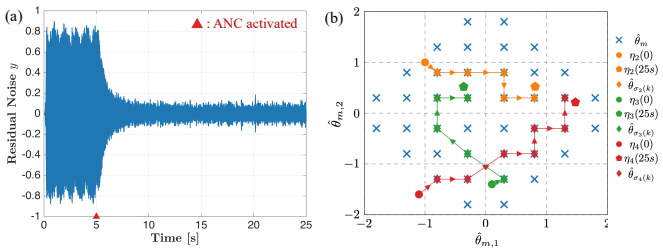

Fig. 4: Composite frequency noise cancellation: (a) noise attenuation efficacy, (b) sequence of switching signals.

MAML, benefiting from pre-trained filter coefficient initial values, achieved comparable suppression effects to our proposed controller. However, MAML fell short of providing comprehensive coverage across the entire frequency spectrum. In contrast, our controller consistently exhibited extension lengths across each frequency direction and a substantial area for composite frequencies, indicating an average composite noise attenuation of approximately -31 dB. Table II further highlights that the proposed controller ensured an average attenuation of about -31 dB with a variance in attenuation of about 0.0743 across distinct frequencies. Additionally, it demonstrated a rapid convergence of 3.7922 seconds. In summary, these findings underscore the effectiveness, versatility, consistency, and superiority of our proposed approach.

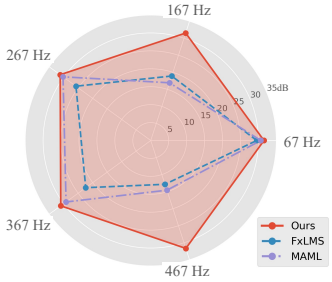

Fig. 5: SOTA comparison for composite noise.

TABLE II: SOTA comparison results.

Method	Avg. Att (dB)	Var. Att	Convg. Time
FxLMS	-21.8904	41.1297	4.9088
MAML	-24.3112	62.0915	**2.6756**
Ours	**-31.3828**	**0.0743**	3.7922

V. Conclusions

This study presents a novel switching-based adaptive feedback ANC for comprehensive multi-sinusoidal noise attenuation in unmodeled environments, ensuring global asymptotic stability, convergence, adaptability of distinct path models, and resilience against some microphone placement errors. This work represents an advancement in noise cancellation techniques compared to SOTAs, offering promising real-world applications. Future research will explore the integration of the proposed controller with the conventional filtered-based methods to achieve narrow band noise attention with the completely cancellation at specfic frequencies.

REFERENCES

[1] P. A. Nelson and S. J. Elliott, *Active control of sound*. Academic Press, 1991.

[2] J. Borenstein and Y. Koren, "Noise rejection for ultrasonic sensors in mobile robot applications," in *Proc. IEEE Int. Conf. Robot. Autom.*, 1992, pp. 1727–1732.

[3] J. Furusho, G. Zhang, and M. Sakaguchi, "Vibration suppression control of robot arms using a homogeneous-type electrorheological fluid," in *Proc. IEEE Int. Conf. Robot. Autom.*, vol. 4, 1997, pp. 3441–3448.

[4] L. Ott, F. Nageotte, P. Zanne, and M. de Mathelin, "Physiological motion rejection in flexible endoscopy using visual servoing and repetitive control : Improvements on non-periodic reference tracking and non-periodic disturbance rejection," in *Proc. IEEE Int. Conf. Robot. Autom.*, 2009, pp. 4233–4238.

[5] S. M. Kuo and D. R. Morgan, *Active noise control systems: algorithms and DSP Implementations*. New York: Wiley, 1996.

[6] S. Wang, H. Li, P. Zhang, J. Tao, H. Zou, and X. Qiu, "An experimental study on the upper limit frequency of global active noise control in car cabins," *Mech. Syst. Signal Process.*, vol. 201, p. 110672, 2023.

[7] S. Kim and M. E. Altinsoy, "A complementary effect in active control of powertrain and road noise in the vehicle interior," *IEEE Access*, vol. 10, pp. 27 121–27 135, 2022.

[8] N. Kwon, M. Park, H.-S. Lee, J. Ahn, and M. Shin, "Construction noise management using active noise control techniques," *J. Constr. Eng. Manag.*, vol. 142, no. 7, p. 04016014, 2016.

[9] Y. Hinamoto and H. Sakai, "A filtered-x lms algorithm for sinusoidal reference signals—effects of frequency mismatch," *IEEE Signal Process. Lett.*, vol. 14, no. 4, pp. 259–262, 2007.

[10] G. Chen and K. Muto, "A theoretical study of convergence characteristics of a multiple channel anc system," *Int. J. Acoust. Vib.*, vol. 9, no. 4, pp. 191–197, 2004.

[11] D. Shi, W.-S. Gan, B. Lam, and S. Wen, "Feedforward selective fixed-filter active noise control: Algorithm and implementation," *IEEE/ACM Trans. Audio Speech Lang. Process.*, vol. 28, pp. 1479–1492, 2020.

[12] M. Tufail, S. Ahmed, M. Rehan, and M. T. Akhtar, "A two adaptive filters-based method for reducing effects of acoustic feedback in single-channel feedforward anc systems," *Digit. Signal Process.*, vol. 90, pp. 18–27, 2019.

[13] S. D. Stearns, *Of aldapfive signal processing*, 1985.

[14] J. Lorente, M. Ferrer, M. de Diego, and A. Gonzalez, "The frequency partitioned block modified filtered-x nlms with orthogonal correction factors for multichannel active noise control," *Digit. Signal Process.*, vol. 43, pp. 47–58, 2015.

[15] D. Shi, W.-S. Gan, B. Lam, and C. Shi, "Two-gradient direction fxlms: An adaptive active noise control algorithm with output constraint," *Mech. Syst. Signal Process.*, vol. 116, pp. 651–667, 2019.

[16] D. Shi, W.-S. Gan, B. Lam, and X. Shen, "Optimal penalty factor for the mov-fxlms algorithm in active noise control system," *IEEE Signal Process. Lett.*, vol. 29, pp. 85–89, 2021.

[17] Z. Luo, D. Shi, and W.-S. Gan, "A hybrid sfanc-fxnlms algorithm for active noise control based on deep learning," *IEEE Signal Process. Lett.*, vol. 29, pp. 1102–1106, 2022.

[18] T.-B. Airimitoaie, I. D. Landau, R. Melendez, and L. Dugard, "Algorithms for adaptive feedforward noise attenuation—a unified approach and experimental evaluation," *IEEE Trans. Control Syst. Technol.*, vol. 29, no. 5, pp. 1850–1862, 2020.

[19] C.-Y. Chang, S. M. Kuo, and C.-W. Huang, "Secondary path modeling for narrowband active noise control systems," *Appl. Acoust.*, vol. 131, pp. 154–164, 2018.

[20] Y. Ma, Y. Xiao, B. Huang, T. Bai, and X. Tan, "A robust feedback active noise control system with online secondary-path modeling," *IEEE Signal Process. Lett.*, vol. 29, pp. 1042–1046, 2022.

[21] P. A. Lopes and J. A. Gerald, "Auxiliary noise power scheduling algorithm for active noise control with online secondary path modeling and sudden changes," *IEEE Signal Process. Lett.*, vol. 22, no. 10, pp. 1590–1594, 2015.

[22] Z. Luo, D. Shi, X. Shen, J. Ji, and W.-S. Gan, "Gfanc-kalman: Generative fixed-filter active noise control with cnn-kalman filtering," *IEEE Signal Process. Lett.*, 2023.

[23] C. Shi, F. Du, C. Liu, and H. Li, "Differential error feedback active noise control with the auxiliary filter based mapping method," *IEEE Signal Process. Lett.*, vol. 29, pp. 573–577, 2022.

[24] T. Saramäki, *Finite impulse reponse filter design*. John Wiley & Sons, 1993, pp. 155–277.

[25] L. V. Wang, W.-S. Gan, A. W. H. Khong, and S. M. Kuo, "Convergence analysis of narrowband feedback active noise control system with imperfect secondary path estimation," *IEEE Trans. on Audio, Speech, and Lang. Process.*, vol. 21, no. 11, pp. 2403–2411, 2013.

[26] L. Wu, X. Qiu, and Y. Guo, "A generalized leaky fxlms algorithm for tuning the waterbed effect of feedback active noise control systems," *Mech. Syst. Signal Process.*, vol. 106, pp. 13–23, 2018.

[27] D. Shi, W.-S. Gan, B. Lam, and K. Ooi, "Fast adaptive active noise control based on modified model-agnostic meta-learning algorithm," *IEEE Signal Process. Lett.*, vol. 28, pp. 593–597, 2021.

[28] G. He, Y. Wang, G. Pin, A. Serrani, and T. Parisini, "Switching-based adaptive output regulation for uncertain systems affected by a periodic disturbance," in *Proc. Amer. Control Conf. (ACC)*, 2022.

[29] M. Bin, D. Astolfi, and L. Marconi, "About robustness of control systems embedding an internal model," *IEEE Trans. Autom. Control*, vol. 68, no. 3, pp. 1306–1320, 2023.

[30] D. R. Morgan, "History, applications, and subsequent development of the fxlms algorithm [dsp history]," *IEEE Signal Process. Mag.*, vol. 30, no. 3, pp. 172–176, 2013.